ORIGINAL ARTICLE

# The effect of waste-expanded perlite on alkali activation of ground granulated blast furnace slag

Sylwia Kucharczyk · Waldemar Pichór

**Abstract** The purpose of this study was to evaluate the possibility of using ground waste-expanded perlite (WP) as a sustainable replacement for ground granulated blast-furnace slag (GGBFS) precursor in alkali-activated systems. The nature and amount of hydration products, microstructure, and compressive strength development were investigated in mixtures where GGBFS was substituted with 10, 20 and 40% by weight of WP and activated by two alkali activators: sodium carbonate and sodium hydroxide. The results show that WP can be successfully used as a partial replacement for GGBFS in alkali-activated materials. Activation by the $Na_2CO_3$ solution was more profitable in terms of compressive strength than NaOH, as well as the amount of water bound in the hydration products was higher. Substitution of GGBFS with 20 wt.% of WP activated with sodium carbonate resulted in a compressive strength of 93 MPa at 90 days of hydration while for the equivalent sample activated by sodium hydroxide, 29 MPa. Further incorporation of WP into $Na_2CO_3$ activated systems resulted in a reduction in performance development, especially at the early age. In addition to C–S–H, hydrotalcite, and three different types of carbonates in the samples activated by NaOH solution, a rich in sodium C(–N)–S–H was found.

## 1 Introduction

Portland cement is the most widely used material for concrete production. Its annual manufacturing is approximately 4200 Mt, generating about 8% of total $CO_2$ [1]. Due to environmental anxiety about $CO_2$ emission, many different "alternative binders" are offered to partially replace ordinary Portland cement (OPC) [2]. Among others, alkali-activated materials (AAMs) are the most renowned. The AAMs based on ground granulated blast-furnace slag (GGBFS) as a precursor represent a vast majority, which is economically and environmentally supported. Production of 1 ton of GGBFS consumes 1300 MJ of energy while producing only 0.07 ton of $CO_2$. However, one should consider that a large proportion of good quality GGBFS and other traditional supplementary cementitious materials (SCMs) are already fully used in the construction industry sector. Therefore, new solutions

S. Kucharczyk (✉) · W. Pichór
Department of Building Materials Technology, Faculty of Materials Science and Ceramics, AGH University of Science and Technology, Al. Mickiewicza 30, 30-059 Kraków, Poland
e-mail: kuchar@agh.edu.pl

W. Pichór
e-mail: pichor@agh.edu.pl

adapting novel, sustainable by-products are invaluable.

The use of expanded perlite as construction material is primarily determined by its physical properties. The cellular microstructure created as a result of rapid heating of Si-Al volcanic rock (perlite) rich in alkalis and approximately 5% of entrapped water induce low bulk density and high porosity. Therefore, its main application route is material for thermal insulation with high thermal [3–5], noise [6] and fire resistance [7] properties. It can be used as a total or partial replacement of natural aggregates (fine or coarse) in concretes, giving lightweight concretes and concretes/mortars with reduced densities [3, 4, 8, 9]. More recently, expanded perlite was used to decrease the thermal conductivity of calcium sulfo-aluminate-based mortars [10].

The production and processing of expanded perlite results in the generation of waste dust, mixed with the residual of uncrushed, cellular expanded perlite. The perlite expansion line is equipped with a cyclones and filters where expanded waste perlite (WP) is collected. Similarly to expanded perlite, perlite waste (WP) is characterized by a high surface area and extremly low bulk density therefore it is challenging to either dispose or store; the chemical and phase composition remains unchanged as well. The processed perlite waste was previously used in autoclaved aerated concrete [11], as a supplementary cementitious material [12–15] as well as a Type II mineral additive to concrete according to the EN 206 standard [16] that shows high pozzolanic properties. High pozzolanic activity results in refinement of capillary porosity, therefore, observed compressive strengths exceed the reference samples without WP addition already beyond 7 days of curing, and the durability is enhanced as well.

Alkali activation is a process of primarily dissolution of the precursor, e.g. GGBFS, at a high pH provided by the alkaline activator followed by condensation reaction and exchange of dissolved species to form the main binding phase C(–N)–A–S–H and other phases depending on the activator used [17–23]. Among the many alkali activators [24] the most attention is focused on sodium hydroxide and sodium silicate with a different ratio of $SiO_2/Na_2O$ for the activation of GGBFS [17, 20–22, 24, 25]. Sodium carbonate is less common, mainly due to frequently reported extended setting times compared to other sodium hydroxide or sodium silicate [19, 25, 26]. However, recent research shows that the fast setting is dependent on the chemical composition and fineness of GGBFS [27–30]. In addition, the sodium carbonate activator is less expensive, more environmentally friendly and is considered easier and safer to operate due to the lower pH value when dissolved in water compared to the widely used activators [31–33].

While the most of the studies on WP focus on employing WP in a traditional cementitious composite exploring mainly hydration (pozzolanic activity), mechanical performance and ecological aspects of using waste material, there is very little data concerning alkali activation in GGBFS-WP systems. Most of the studies conducted so far concentrate on activation by using water glass or combination of NaOH and waterglass. Research has shown [34] that the substitution of GGBFS by 10, 30 and 50 vol. % of perlite activated waste activated by a mixture of sodium silicate with a NaOH solution results in at most a 16% decrease in compressive strength compared to the reference sample without the addition of perlite, however, the strength at 28 days reaches the level of 45–65 MPa, which proves its suitability and applicability as a binder. Moreover, less heat was released, limiting the risk of cracking observed in pure alkali activated slag [35].

The main objective of the presented research is upper limit utilization of the waste expanded perlite in the material that can develop mechanical strength and performance comparable to Portland cement, is cost-effective and has low-environmental footprint e.g. in alkali-activated slag. Moreover the GGBFS-WP system gives possibilities to further explore the effect of GGBFS substitution by waste WP in highly alkaline environment provided by NaOH and $Na_2CO_3$ solutions which are employed for the first time in such binders. Substitution level of GGBFS by WP increases systematically by 10, 20 and 40 wt.% to on the one hand utilize maximum level of WP while keeping GGBFS-WP binder (not vice versa) and on the other hand to check in which point the final material retains its positive qualities. The compressive strength of GGBFS-WP pastes is analyzed at the curing ages of 1, 3, 7, 14, 28, 56 and 90 days and the reaction products are characterized using X-ray diffraction (XRD), thermogravimetry analysis (TGA) and Fourier-transform infrared spectroscopy (FT-IR). The amount of water bound in hydration products is calculated from

TGA results and microstructure accessed from scanning electron microscope (SEM) images.

## 2 Materials and sample preparation

As primary row material, a ground granulated blast-furnace slag (GGBFS) and ground waste-expanded perlite, hereafter named waste perlite (WP), with the chemical composition given in Table 1 were used. The slag is characterized by a relatively low content of $Al_2O_3$ and MgO. Its specific gravity is 2800 kg/m$^3$ with a Blaine fineness of 520 m$^2$/kg. The WP is an amorphous component consisting mainly of $SiO_2$ and $Al_2O_3$ ($SiO_2 + Al_2O_3 = 88.7$ wt.%), and alkalis ($^{*}$-$Na_2O_{eq} = 6.1$). It is characterized by a low bulk density (200 kg/m$^3$) due to its cellular microstructure. Therefore, before use, the WP was pelletized by pre-pressing in steel cylinders of 20 mm diameter with 200 kN force. The pellets were subsequently ground in a laboratory ball mill for 2 h to improve its physical properties and increase bulk density. As a result, a

**Table 1** Chemical composition (XRF, wt.%) of the GGBFS and WP

| Chemical composition (wt.%) | | |
|---|---|---|
|  | GGBFS | WP |
| CaO | 42.36 | 0.5 |
| $SiO_2$ | 38.02 | 76.2 |
| $Al_2O_3$ | 7.02 | 12.5 |
| $Fe_2O_3$ | 0.87 | 1.3 |
| MgO | 6.87 | 0.7 |
| MnO | 0.45 | – |
| $Na_2O$ | 0.77 | 3.1 |
| $K_2O$ | 0.48 | 4.5 |
| $SO_3$ | 1.21 | – |
| $P_2O_5$ | 1.06 | – |
| $TiO_2$ | 0.39 | 0.35 |
| $^{*}Na_2O_{eq}$ | 1.1 | 6.1 |
| LOI (1050 °C) | 0.18 | 0.6 |
| Sum | 99.68 | 99.80 |
| Specific density [g/cm$^3$] | 2.8 | 2.4 |
| $d_{10}$ [μm] | 1.6 | 0.8 |
| $d_{50}$ [μm] | 11 | 6 |
| $d_{90}$ [μm] | 40 | 20 |

$^{*}Na_2O_{eq} = Na_2O + 0{,}658\ K_2O$

finely ground material was achieved. Some physical parameters of GGBFS and WP are given in Table 1. Two types of reagent-grade activators were used: sodium carbonate (C) and sodium hydroxide (N). 5% of each activator relative to the mass of the slag to give a final $Na_2O$ content of 2.9 and 3.9 sodium carbonate and sodium hydroxide, respectively.

To examine the influence of perlite on sodium carbonate and sodium hydroxide activated slag, 10, 20 and 40 wt.% of the GGBFS were replaced by WP. The reference sample was pure alkali-activated slag. Before preparing the pastes dry components (GGBFS and WP) were homogenized for 2 h in plastic containers with five rubber stoppers of different size. To prepare paste samples, the appropriate amount of sodium carbonate and sodium hydroxide was dissolved in distilled water prior to mixing in order to obtain a homogenous distribution. The quantity of water necessary to make the pastes was experimentally determined during preliminary prism-forming tests. All pastes showed similar consistency at the water to binder ratio (w/b) of 0.5. The composition of the prepared GGBFS and GGBFS-WP mixes is presented in Table 2. The reference samples are designated by the kind of alkali-activator used to the GGBFS (C – $Na_2CO_3$, N – NaOH) and the amount of WP that replace GGBFS is marked as 10WP, 20WP, 40WP therefore e.g. C10WP is the sample of GGBFS with 10 wt.% of WP activated by $Na_2CO_3$.

## 3 Methods

The samples required for XRD, TGA and FT-IR were thoroughly mixed with a hand mixer for 2 min and placed in plastic vials. For XRD, TGA, and FT-IR measurements after designated time (7, 28 and 56 days) a piece of the sample was cut, ground in agate mortar, sieve through 63 μm and dried in a vacuum desiccator over silica gel until a constant weight was achieved (changes of mass are less than 0.1% of the sample per day).

XRD was performed on the Philips X'Pert X-ray diffractometer system and CuKα radiation ($\alpha = 1.54$ Å). The samples were scanned in an angular range of 3–60° with a steep size of 0.05° and a time per step of 2 s.

TGA was obtained in approximately 90 mg of the powder sample using a corundum crucible and

**Table 2** Mix design (wt.%)

| Compound | C | C10WP | C20WP | C40WP | N | N10WP | N20WP | N40WP |
|---|---|---|---|---|---|---|---|---|
| GGBFS | 100 | 90 | 80 | 60 | 100 | 90 | 80 | 60 |
| WP | – | 10 | 20 | 40 | – | 10 | 20 | 40 |

w/b = 0.5

analyzed with STA 449F3 Jupiter by Netzsch. The tests were carried out in a temperature range of 30 to 1000 °C at 10 °C/min in a helium atmosphere with a gas flow of 20 ml/min. The amount of bound water (%BW) is calculated according to the equation %BW = $((m_{75} - m_{450})/m_{450})$ 100 where m is designated to the mass of the sample at 75 °C and 450 °C respectively.

FT-IR was conducted in the mid-infrared range (4000–400 cm$^{-1}$) on a Bruker Optics-Vertex70V spectrometer. The tests were performed with the transmission technique using standard KBr pellets. Spectra were recorded with a resolution of 4 cm$^{-1}$ and 256 scans.

For SEM investigations, a piece of the fresh sample at 56 days of hydration was coated with a carbon layer. The topography of the sample was examined at a magnification of 10 000 × to 20 000 × using FEI Nova NanoSem 200 scanning electron microscopy.

For compressive strength experiments, alkali activated GGBFS and GGBFS-WP pastes prepared according to the same methodology as for XRD, TGA, FT-IR and SEM were casted in 25 mm × 25 mm × 100 mm prisms. Curing of the sample and compressive strength tests were performed according to the PN-EN 196-1 however with lower loading rate 0.5 kN/s. After 24 h, the samples were demolded and cured in water at 20 ± 1 °C. The compressive strength was determined after 1, 3, 7, 14, 28, 56 and 90 days of hydration. Each testing age was performed on 6 prisms.

# 4 Results and discussion

## 4.1 Raw materials

### 4.1.1 XRD and SEM

Both GGBFS and WP are entirely amorphous, as no peaks are observed on the diffractograms in Fig. 1. An observed maximum of diffuse scattering characterizes the short-range order of the materials. The clear
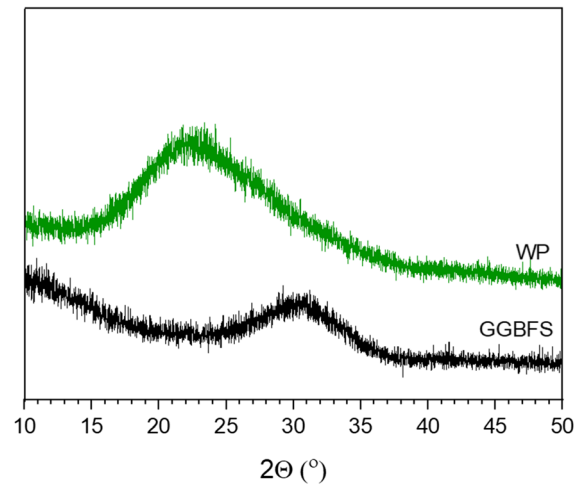


**Fig. 1** XRD scans of GGBFS and WP

change in the 'hump' between GGBFS and WP is related to their chemical composition [36], more specifically, the high silica content in WP induces a 'hump' at lower angle (maximum at 23 2Θ), as the ratio of CaO/SiO$_2$ increases in GGBFS the 'hump' moves to higher angle (maximum at 31 2Θ). The microstructure of WP before and after grinding is presented in Fig. 2.

## 4.2 Alkali activated pastes

### 4.2.1 XRD

The results of samples with 20% WP activated by Na$_2$CO$_3$ (Fig. 3a) show reflection of the C–S–H phase, hydrotalcite (Mg-containing LDH phase) and three types of carbonates: two polymorphs of CaCO$_3$ – vaterite and calcite and hydrated double salt – gaylussite (Na$_2$Ca(CO$_3$)$_2$•5H$_2$O). Carbonate formation at the early time of hydration (7 days) may suggest a preferential reaction of dissolved CO$_3$$^{2-}$ and calcium derived from dissolved slag [19]. Vaterite and calcite visible at later ages may also occur due to carbonation of the sample. For the samples activated by NaOH solution (Fig. 3b) XRD results reveal the presence of rich sodium C(–N)–S–H (7 2Θ) in
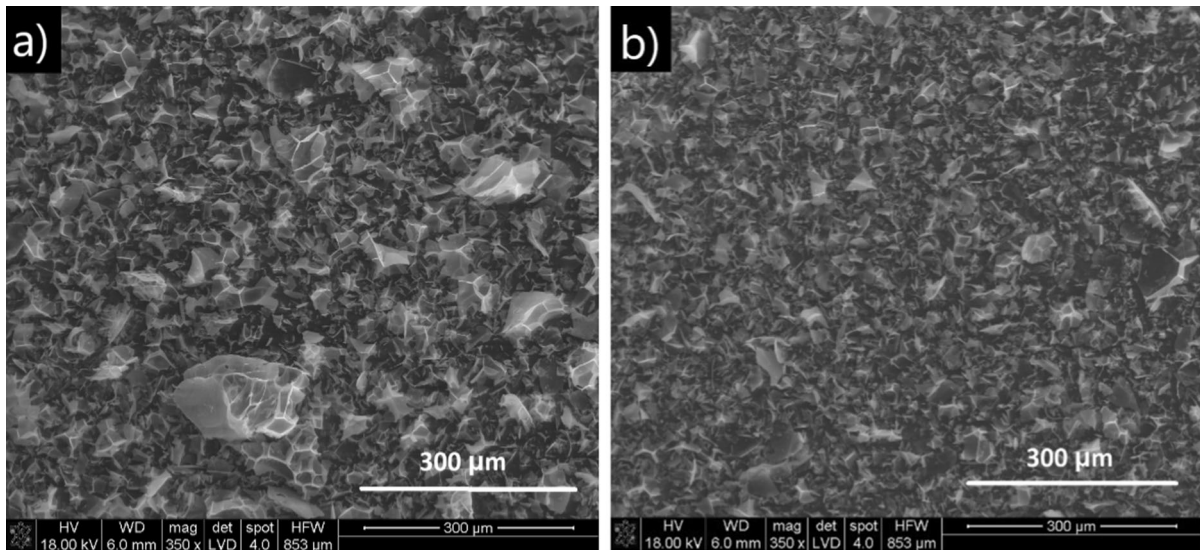
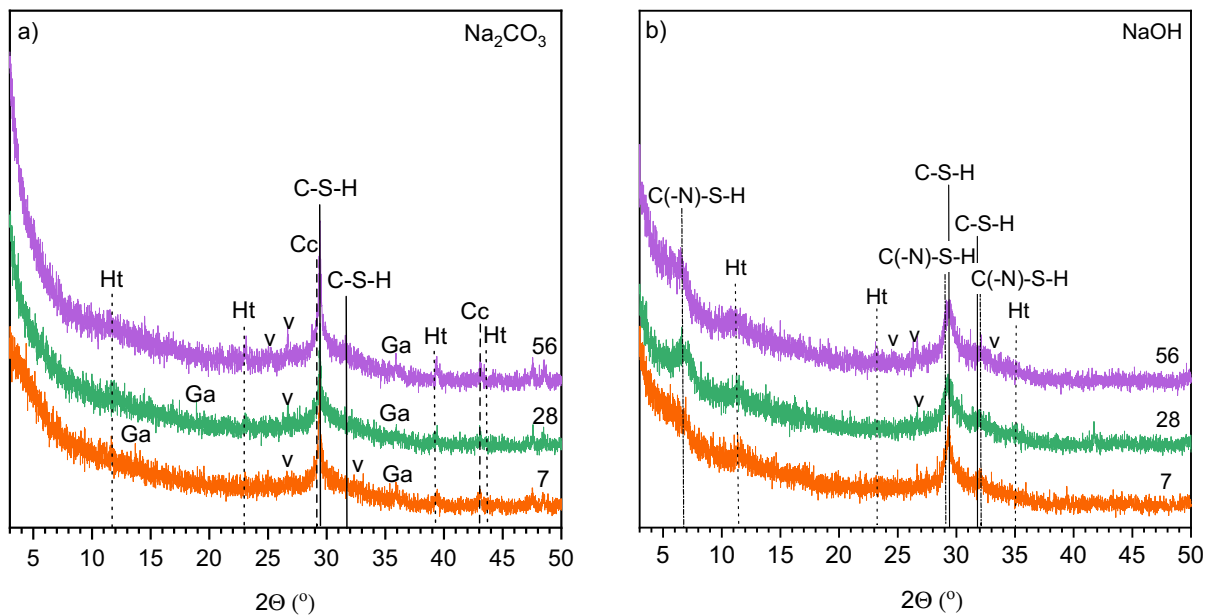**Fig. 2** WP a) before and b) after grinding



**Fig. 3** Comparison of XRD patterns of a) $Na_2CO_3$ and b) NaOH activated GGBFS with 20 wt.% of perlite at 7, 28 and 56 days of curing. C–S–H - C–S–H phase, C(–N)–S–H - sodium rich C–S–H, Ht - hydrotalcite, Ga - gaylussite, Cc - calcite, v - vaterite

addition to C–S–H, hydrotalcite, vaterite, and calcite. The C(–N)–S–H phase in NaOH slag activated samples is characterized by a more dense (containing less water—inner) and more crystalline structure [20, 22]. No major differences were observed between the diffractograms of the samples with hydration time independently of the type of activator used. Moreover,

regardless of the activation method, no zeolites were observed in the samples as reported elsewhere [37].

The gradual addition of WP does not change the nature of the hydration products, as can be observed in Fig. 4. However, an effect of WP presence and hence slightly changed chemistry of the samples is visible; e.g. crystalline products such as hydrotalcite present
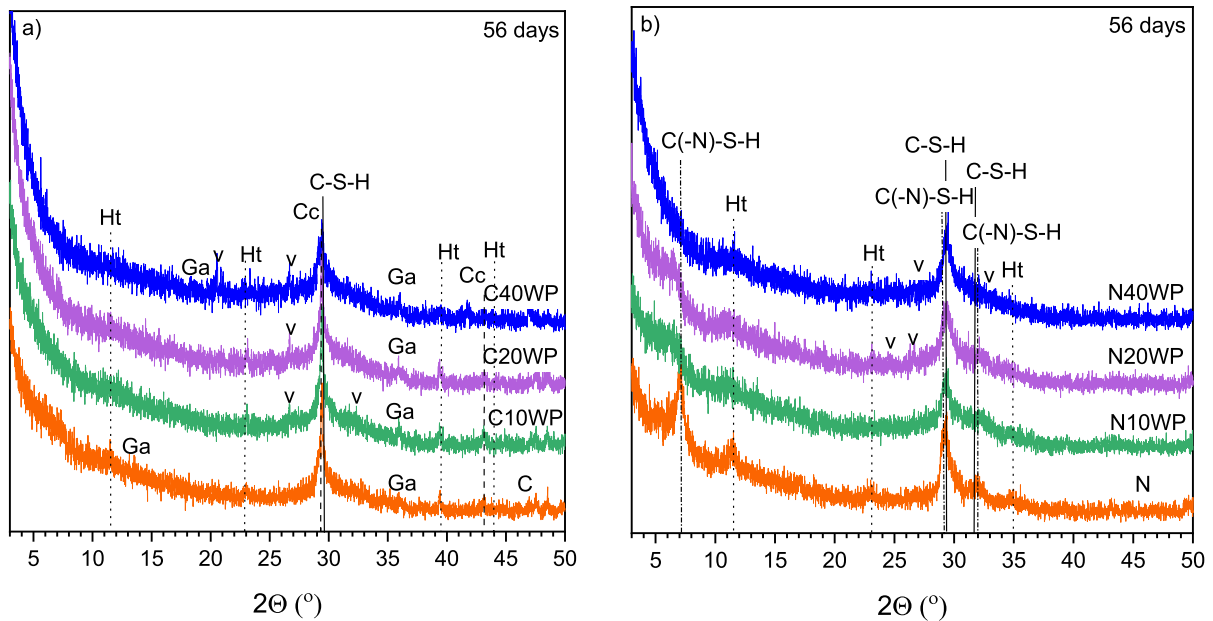
**Fig. 4** Comparison of XRD patterns of a $Na_2CO_3$ and b NaOH activated GGBFS with different perlite dosage at 56 days of curing. C–S–H - C–S–H phase, C(–N)–S–H - sodium rich C–S–H, Ht - hydrotalcite, Ga - gaylussite, Cc - calcite, v - vaterite

for pure samples (especially the N sample Fig. 4b) become less pronounced. This is due to the reduction of the concentration of MgO in the samples containing WP. Similarly, the peak related to C(–N)–S–H clearly weakens (Fig. 4b) and that related to C–S–H is more noticeable. It may suggest that when WP is present as a result of the change in chemistry of the system, a lower C–S–H ratio is formed, the system is less prone to sodium, and it is more susceptible to aluminum uptake, resembling more fly ash activated systems.

### 4.2.2 TGA

The TGA result presented in Fig. 5 is in agreement with the phase identification by XRD analysis (Figs. 3 and 4). Mass loss at temperatures below 200 °C can be attributed to free water removal and the initial loss of the interlayer and structural water present in C–S–H and C(–N)–S–H [38]. The decomposition of hydrotalcite exhibits a double-step dehydration process at 200 °C and 350 °C [23, 38]. More hydrotalcite precipitation was observed in the reference samples without WP addition, which is the result of a higher overall MgO content in the sample. The broad effects observed mainly for the sodium carbonate activated samples, beginning at approximately 450 °C, are

related to the $CO_2$ loss from carbonate salts. At ∼ 550 °C calcite decomposes, followed by decarbonation of gaylussite, present mainly in $Na_2CO_3$ activated samples [39]. Before gaylussite decarbonate it loses molecules of water at ∼ 130 °C, however this effect is unclear due to overlapping effects with the C–S–H and C(–N)–S–H phase. Despite the fact that the XRD data show the presence of vaterite in the samples, no effect at approximately 390 °C related to the conversion of vaterite to calcite is observed, probably due to low concentration of this phase or due to the coincident with hydrotalcite. Form Figs. 5 and 6 is clear that the amount of products formed increases with hydration time, more hydration products are observed for the samples activated with $Na_2CO_3$ and for those where 20 wt.% of WP is present. The results prove that WP is an active component of the blends.

### 4.2.3 FT-IR

FT-IR was performed to further investigate the change of chemical groups in reaction products.

Figure 7 compares the spectra of the $Na_2CO_3$ and NaOH activated GGBFS and GGBFS-WP blends. All spectra show similar shapes and positions of the bands and are comparable with those previously published
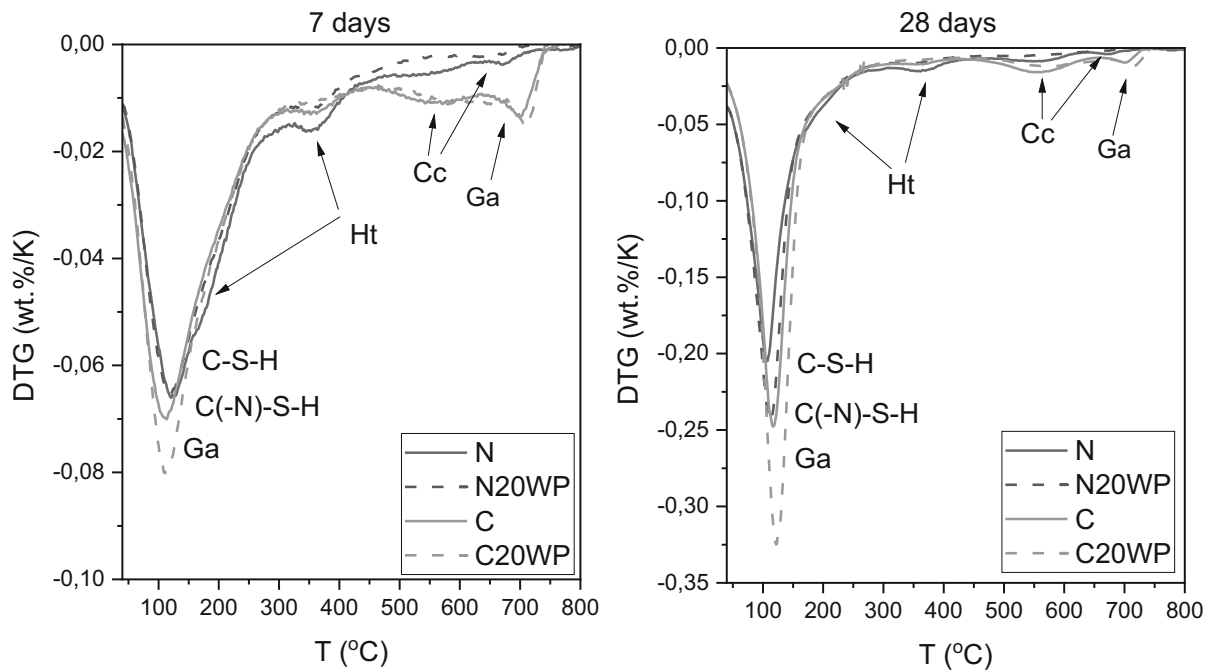
**Fig. 5** Comparison of DTG results for the reference samples and with 20% of WP at 7 and 28 days of hydration (note that for the better visibility the y-axis scale is different for 7 and 28 days results). C–S–H - C–S–H phase, C(–N)–S–H - sodium rich C–S–H, Ht - hydrotalcite, Ga - gaylussite, Cc - calcite
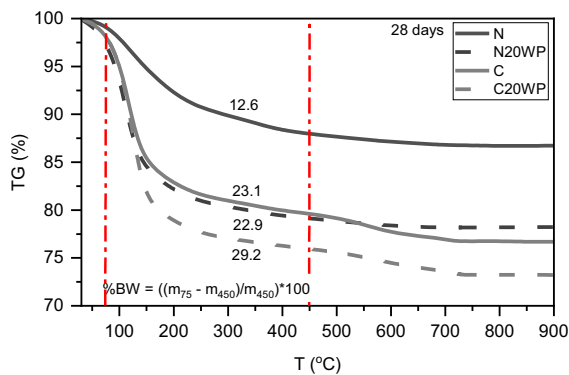


**Fig. 6** The amount of bound water present (%BW) in hydration products of GGBFS and GGBFS with 20 wt.% of WP activated by $Na_2CO_3$ and NaOH at 28 days of hydration

for alkali activated samples [25, 29, 30, 40]. High full with half maximum (FWHM) at $1300 – 800$ $cm^{-1}$ and the band at $670$ $cm^{-1}$ confirms that the investigated samples are highly amorphous. The Si–O–Si stretching vibration mode of the C–S–H and C(–N)–S–H phase is identified at $950–960$ $cm^{-1}$ [41] overlapping resonances from unreacted glassy phase, either from GGBFS (calcium alumina-silicate glass) or WP (alumina-silicate glass). Pure samples (C, N) show the

main band centered at $\sim 950$ $cm^{-1}$. The gradual addition of perlite results in band shifts to higher wavenumbers ($\sim 950$ $cm^{-1} \rightarrow \sim 1000$ $cm^{-1}$). A different wavenumber indicates a different ratio of Si/Ca in calcium-silicate-hydrate phase [42–44]. In this case, the low position indicates the formation of C–S–H with a lower Si/Ca ratio. The band at $670$ $cm^{-1}$ present silico and silico-alumino-oxygen rings derived from the perlite and GGBFS structure [45–47]. A sharp but week band at $\sim 870$ $cm^{-1}$ as well as bands at around $720$ $cm^{-1}$, $1430$ $cm^{-1}$ and $1800$ $cm^{-1}$ more distinct for $Na_2CO_3$ activated samples, are assigned to vibrations of C–O groups from calcite, vaterite and gaylussite. Two bands at $3428$ $cm^{-1}$, $3200$ $cm^{-1}$ represent vibrations in water molecules originating from O–H stretching vibrations and $1646$ $cm^{-1}$ of O–H bending vibrations of interlayer water molecules of C–S–H, C(–N)–S–H, and hydrotalcite [48]. The bands observed at approximately $424$ $cm^{-1}$ and $542$ $cm^{-1}$ are associated vibrations O–Al(Mg)–O and Al(Mg)–O–Al octahedra [49, 50] respectively in layer structured hydrotalcite. The bands in this region were previously attributed to AFm phases and its dehydration products [51] and monocarbonate [49].
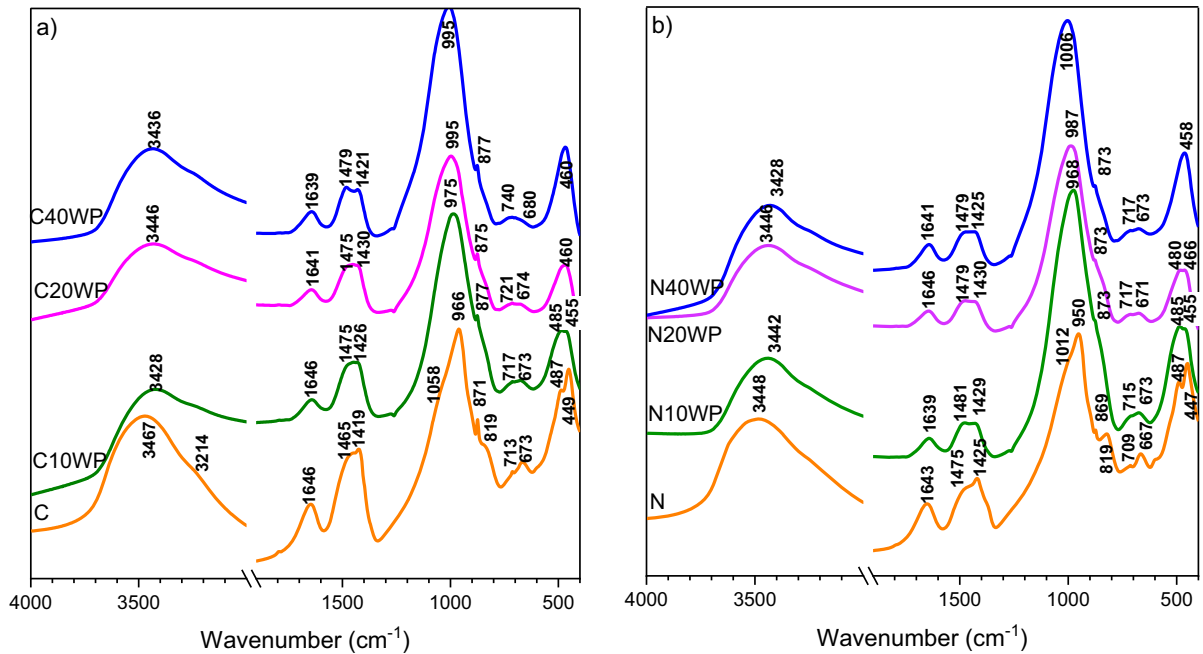
**Fig. 7** Comparison of IR spectra of a) $Na_2CO_3$ and b) NaOH activated GGBFS with different perlite dosage at 56 days of curing

### 4.2.4 SEM

Figures 8 and 9 shows the SEM pictures of the reference samples and the samples with 20 and 40 wt.% replacement of GGBFS by WP at the curing age of 28 days. The morphology of the reference samples (Figs. 8a, d, 9a and d) is clearly different from that of the samples containing WP. As can be seen, the morphology of the C mixture (Figs. 8a and 9a) appears to be more compact and dense, while the N sample (Figs. 8d and 9d) is rich in a semi-crystalline structure embedded in the matrix, which is likely to be C(–N)–S–H phase as revealed by the XRD (Fig. 4b). The addition of 20 wt.% of perlite positively influences the microstructure of both alkali-activated series (Figs. 8b, e, 9b and e). The images show mainly C–S–H phase growing on the well-reacted grains of GGBFS and WP. In the case of the NaOH activated sample, the increase in the amount of WP to 40 wt.% (Figs. 8f and 9f) appears to not influence the microstructure in comparison to the N20WP blend (Figs. 8e and 9e), while the microstructure of C40WP (Figs. 8c and 9c) became more porous and the grains are more distinct (less reacted) in comparison to the C20WP sample (Figs. 8b and 9b).

### 4.2.5 Compressive strength

The results clearly show that the compressive strength of the pastes strongly depends on the type of activator used, as well as the mass proportion of GGBFS and WP (Figs. 10, 11, 12). In general, higher strengths are observed in both the reference paste and GGBFS-WP when $Na_2CO_3$ instead of NaOH is used. Despite the lower pH value of the $Na_2CO_3$ solution, the initial reaction delay reported elsewhere [19, 25, 26] for the $Na_2CO_3$ activated GGBFS sample (C) is not noticed, and the strengths are higher than for the NaOH activated reference sample (N). The lower activation ability at early age is often combined with the preferential reaction of $Ca^{2+}$ from GGBFS dissolution with $CO_3^{2-}$ from the activator to form calcium carbonates and gaylussite that do not give strength [19, 25, 29]. However, a fast setting of GGBFS activated by $Na_2CO_3$ is also reported [27–30]. Yuan et al. [29] found that the early development of the strength of $Na_2CO_3$ activated GGBFS is significantly controlled by the fineness of the slag particles. The reduction of the slag particles size increases the strength due to the acceleration of formation of the strength giving phases. The strengths of the reference sample (C) gradually grow up to 14 days; after this,
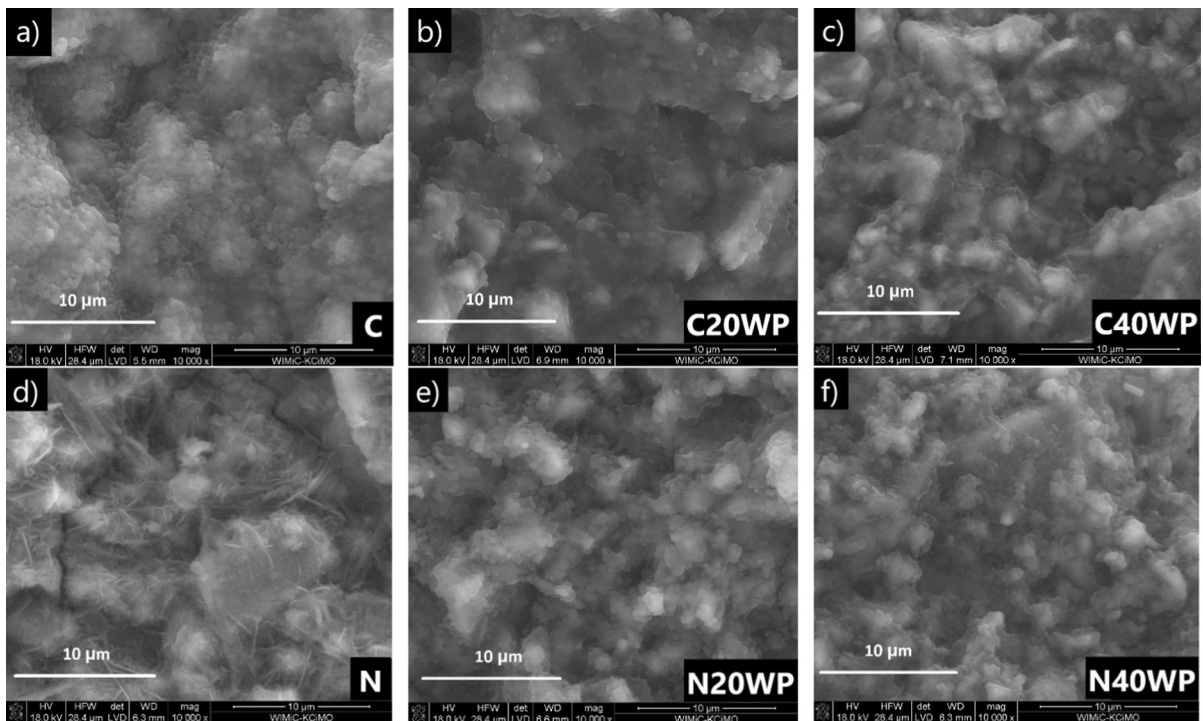
**Fig. 8** SEM images of the reference samples (a and d) and GGBFS blends with 20 (b and e) and 40 wt.% (c and f) of WP activated by Na$_2$CO$_3$ (a, b and c) and NaOH (d, e and f) solutions at 56 days of hydration and magnification 10 000x

there is an ongoing gradual increase in compressive strength with prolonged curing (43 MPa at 90 days of curing). The higher strengths of the C series at later ages is assigned to the effect of the anion CO$_3{}^{2-}$ [26]. The addition of WP to the Na$_2$CO$_3$ activated systems results in an initial delay in the early reaction time and the samples did not set until 3 days after curing (Fig. 10). From 3 days and on, the addition of 10 wt.% and 20 wt.% of WP to the GGBFS boosts the reaction and compressive strength is higher than for the reference sample. The low alkalinity of the system is probably insufficient to trigger the reaction of GGBFS-WP at early ages. Later, the dissolved WP silicate species reacts favorably instead of the GGBFS aluminosilicates with the Na$^+$ cations of the activator, forming more hydration products (Fig. 6) that give strength. The optimum of WP substitution in Na$_2$CO$_3$ activated samples is 20%, at 28 days the compressive strength is 72 MPa and at 90 days 93 MPa (Figs. 10 and 12). 40% of WP clearly slows down the reaction; however, at 90 days the compressive strength surpasses the samples with 10% of WP (Figs. 10 and 12). It may suggest that there are not enough Na$^+$ ions left

to react with dissolved GGBFS because of a high proportion of WP in the blend.

Regarding the NaOH activated GGBFS-WP series, the initial reaction delay is not observed, most probably due to higher alkalinity of the NaOH solution. The influence of WP on the activated NaOH samples is twofold (Figs. 11 and 12). 10 wt.% of the WP results in decrease of compressive strength throughout the studied period compared to the reference sample. Addition of 20 wt.% and 40 wt.% of WP to the GGBFS causes an increase in compressive strength. In the set of NaOH activated GGBFS-WP samples, 40 wt.% WP addition is the most favorable independently on the time of curing (Figs. 11 and 12). The differences in compressive strength between the samples in NaOH activated series are most likely due to the different dissolution rates of GGBFS and WP and their reactions mechanisms in a highly alkaline environment, e.g. reaction of alkaline activation and/ or geopolimerization. However, this divagation is out of scope of this paper.
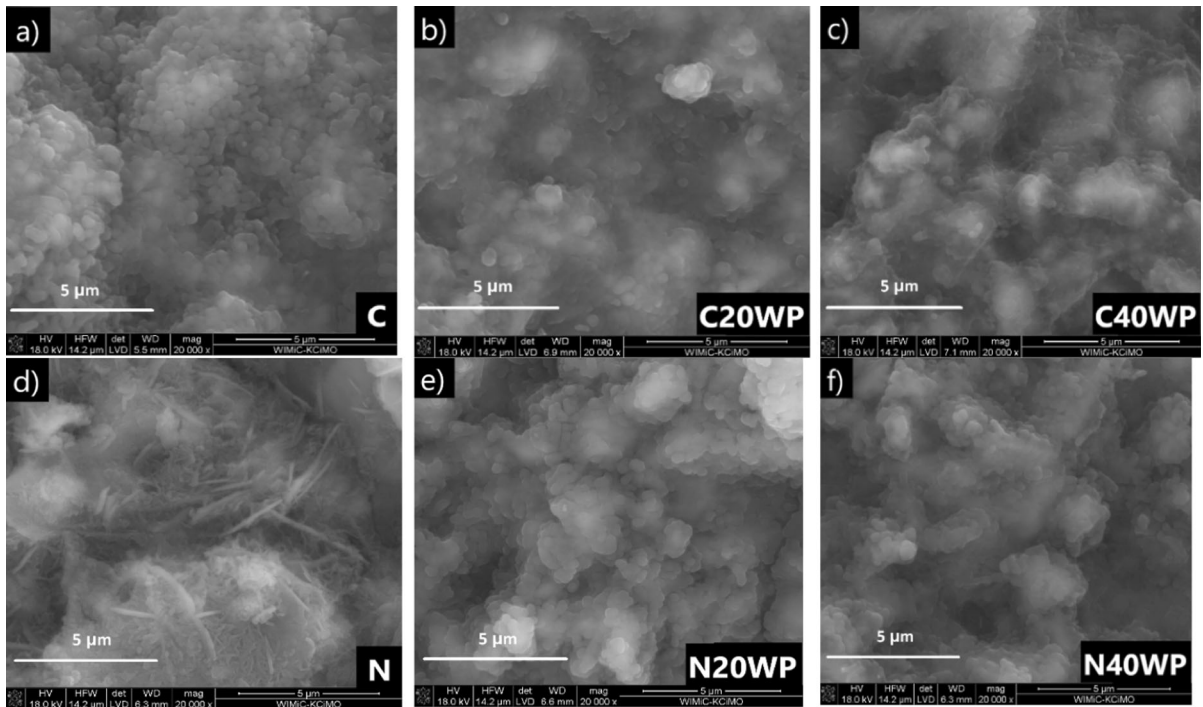
**Fig. 9** SEM images of the reference samples (a and d) and GGBFS blends with 20 (b and e) and 40 wt.% (c and f) of WP activated by $Na_2CO_3$ (a, b and c) and NaOH (d, e and f) solutions at 56 days of hydration and magnification 20 000x
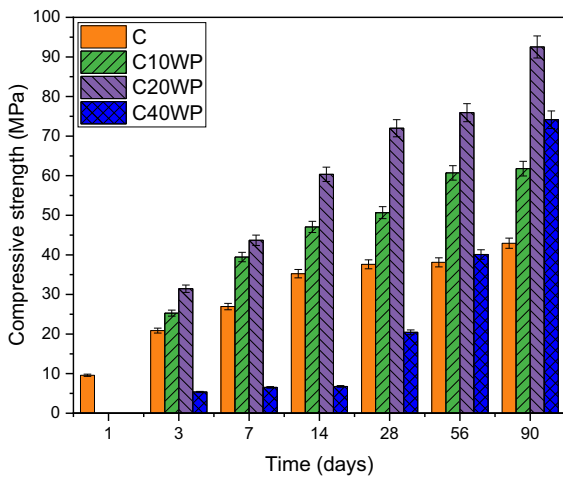


**Fig. 10** Compressive strength of $Na_2CO_3$ activated GGBFS with different WP dosage
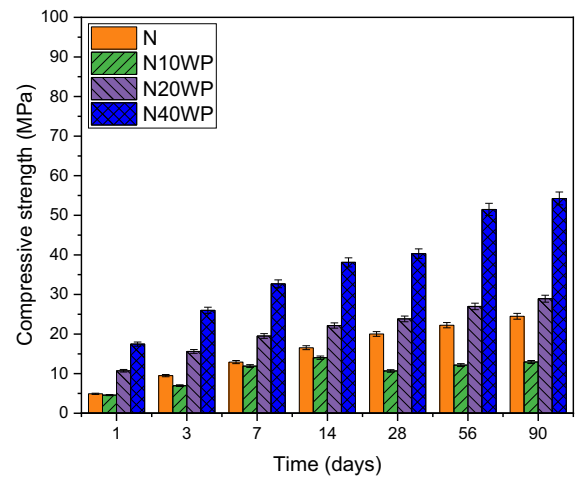


**Fig. 11** Compressive strength of NaOH activates GGBFS with different WP dosage

## 5 Conclusions

The results obtained confirm that WP can be effectively used as a partial replacement of GGBFS in sodium carbonate and sodium hydroxide activated systems. Moreover, the use of WP reduces the consumption of good quality GGBFS, which is practically fully used in common cements, or it allows the use of medium quality GGBFS. The amount of waste stored in the landfill also decreases. The nature of hydration products as revealed by XRD depends mainly on the type of alkali activator used. For
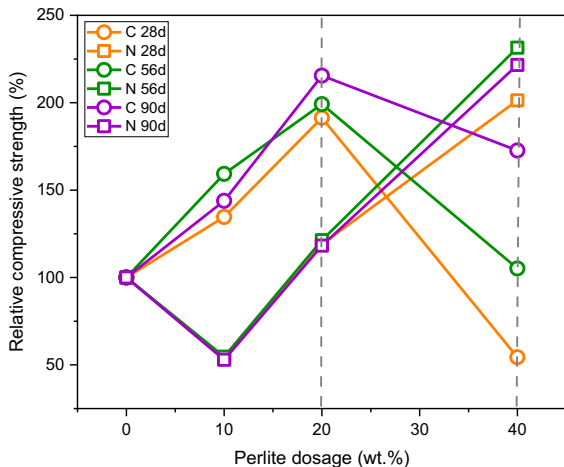
**Fig. 12** Influence of WP dosage on compressive strength of GGBFS-WP alkali activated pastes in relative to neat GGBFS activated samples at 28, 56 and 90 days of curing

$Na_2CO_3$ activated samples, the phases formed during hydration are C–S–H, hydrotalcite, and three types of carbonates: vaterite, calcite, and gaylussite. In the samples activated by NaOH solution, sodium-rich C(–N)–S–H is also observed. WP presence does not change the nature of the hydration products, however a slightly changed chemistry of the samples with WP results in less pronounced C(–N)–S–H and hydrotalcite precipitation. The TG/DTG and FTIR are consistent with the XRD results. The exemplary, simple bound water calculations show that the amount of hydration products is higher in systems activated with $Na_2CO_3$ compared to their NaOH activated equivalents. The analysis of the SEM pictures seems to confirm these results, since the microstructure of the sample activated by sodium carbonate is more compact and dense. The compressive strength of the paste samples depends first on the type of activator and secondly on the GGBFS substitution by WP. Generally, higher compressive strength values are observed for $Na_2CO_3$ activated paste samples, which is in line with BW calculations and microstructure observations. The optimum of the incorporation of WP is 20 wt.% for sodium carbonate giving over 90 MPa at 90 days of hydration. Further substitution results in significantly lower performance, especially at early ages. Only the 1 day samples with WP activated by $Na_2CO_3$ did not set in contrary to NaOH activation probably due to a triggering effect of a higher pH of the NaOH solution. The compressive strength of

NaOH activated systems is higher as the higher is the GGBFS substitution by WP. The differences in compressive strength between two considered systems are presumably the result of different dissolution rates of GGBFS and WP and their mechanisms of reaction in a highly alkaline environment, e.g. reaction of alkaline activation and/or geopolimerization.

**Declarations**

## References

1. Gartner E (2004) Industrially interesting approaches to "low-$CO_2$" cements. Cem Concr Res 34:1489–1498. https://doi.org/10.1016/j.cemconres.2004.01.021
2. Gartner E, Sui T (2018) Alternative cement clinkers. Cem Concr Res 114:27–39. https://doi.org/10.1016/J.CEMCONRES.2017.02.002
3. Topçu IB, Işikdağ B (2008) Effect of expanded perlite aggregate on the properties of lightweight concrete. J Mater Process Technol 204:34–38. https://doi.org/10.1016/J.JMATPROTEC.2007.10.052
4. Sengul O, Azizi S, Karaosmanoglu F, Tasdemir MA (2011) Effect of expanded perlite on the mechanical properties and thermal conductivity of lightweight concrete. Energy Build 43:671–676. https://doi.org/10.1016/J.ENBUILD.2010.11.008
5. Gandage AS, Rao VRV, Sivakumar MVN et al (2013) Effect of perlite on thermal conductivity of self compacting concrete. Procedia Soc Behav Sci 104:188–197. https://doi.org/10.1016/J.SBSPRO.2013.11.111
6. Yilmazer S, Ozdeniz MB (2005) The effect of moisture content on sound absorption of expanded perlite plates. Build Environ 40:311–318. https://doi.org/10.1016/J.BUILDENV.2004.07.004

7. Singh M, Garg M (1991) Perlite-based building materials–a review of current applications. Constr Build Mater 5:75–81. https://doi.org/10.1016/0950-0618(91)90004-5

8. Demirboğa R, Örüng I, Gül R (2001) Effects of expanded perlite aggregate and mineral admixtures on the compressive strength of low-density concretes. Cem Concr Res 31:1627–1632. https://doi.org/10.1016/S0008-8846(01)00615-9

9. Lanzón M, García-Ruiz PA (2008) Lightweight cement mortars: advantages and inconveniences of expanded perlite and its influence on fresh and hardened state and durability. Constr Build Mater 22:1798–1806. https://doi.org/10.1016/J.CONBUILDMAT.2007.05.006

10. Huang G, Pudasainee D, Gupta R, Liu WV (2021) Thermal properties of calcium sulfoaluminate cement-based mortars incorporated with expanded perlite cured at cold temperatures. Constr Build Mater 274:122082. https://doi.org/10.1016/J.CONBUILDMAT.2020.122082

11. Różycka A, Pichór W (2016) Effect of perlite waste addition on the properties of autoclaved aerated concrete. Constr Build Mater 120:65–71. https://doi.org/10.1016/J.CONBUILDMAT.2016.05.019

12. Kotwica Ł, Pichór W, Nocuń-Wczelik W (2016) Study of pozzolanic action of ground waste expanded perlite by means of thermal methods. J Therm Anal Calorim 123:607–613. https://doi.org/10.1007/S10973-015-4910-8

13. Kapeluszna E, Kotwica Ł, Nocuń-Wczelik W (2015) Study of expanded perlite by-product as the mineral addition to Portland cement. Cement Wapno Beton 20:33–44. https://doi.org/10.32047/CWB.2015.20.1.5

14. Kotwica Ł, Pichór W, Kapeluszna E, Różycka A (2016) Utilization of waste expanded perlite as new effective supplementary cementitious material. J Clean Prod. https://doi.org/10.1016/j.jclepro.2016.10.018

15. Kapeluszna E, Kotwica Ł, Nocuń-Wczelik W (2021) Comparison of the effect of ground waste expanded perlite and silica fume on the hydration of cements with various tricalcium aluminate content–Comprehensive analysis. Constr Build Mater 303:124434. https://doi.org/10.1016/J.CONBUILDMAT.2021.124434

16. Łagosz A, Olszowski D, Pichór W, Kotwica Ł (2021) Quantitative determination of processed waste expanded perlite performance as a supplementary cementitious material in low emission blended cement composites. J Build Eng 40:102335. https://doi.org/10.1016/J.JOBE.2021.102335

17. García Lodeiro I, Macphee DE, Palomo A, Fernández-Jiménez A (2009) Effect of alkalis on fresh C-S–H gels. FTIR analysis. Cem Concr Res 39:147–153. https://doi.org/10.1016/J.CEMCONRES.2009.01.003

18. Bernal SA, Provis JL, Walkley B et al (2013) Gel nanostructure in alkali-activated binders based on slag and fly ash, and effects of accelerated carbonation. Cem Concr Res 53:127–144. https://doi.org/10.1016/J.CEMCONRES.2013.06.007

19. Bernal SA, Provis JL, Myers RJ et al (2014) Role of carbonates in the chemical evolution of sodium carbonate-activated slag binders. Mater Struct Materiaux Const 48:517–529. https://doi.org/10.1617/S11527-014-0412-6

20. Ben Haha M, le Saout G, Winnefeld F, Lothenbach B (2011) Influence of activator type on hydration kinetics, hydrate assemblage and microstructural development of alkali activated blast-furnace slags. Cem Concr Res 41:301–310. https://doi.org/10.1016/J.CEMCONRES.2010.11.016

21. Bernal SA, Provis JL, Rose V, Mejía De Gutierrez R (2011) Evolution of binder structure in sodium silicate-activated slag-metakaolin blends. Cem Concr Compos 33:46–54. https://doi.org/10.1016/J.CEMCONCOMP.2010.09.004

22. Ben Haha M, Lothenbach B, le Saout G, Winnefeld F (2011) Influence of slag chemistry on the hydration of alkali-activated blast-furnace slag–Part I: effect of MgO. Cem Concr Res 41:955–963. https://doi.org/10.1016/j.cemconres.2011.05.002

23. Ben Haha M, Lothenbach B, le Saout G, Winnefeld F (2012) Influence of slag chemistry on the hydration of alkali-activated blast-furnace slag–Part II: effect of Al2O3. Cem Concr Res 42:74–83. https://doi.org/10.1016/j.cemconres.2011.08.005

24. Luukkonen T, Abdollahnejad Z, Yliniemi J et al (2018) One-part alkali-activated materials: a review. Cem Concr Res 103:21–34. https://doi.org/10.1016/J.CEMCONRES.2017.10.001

25. Fernandez-Jimenez A, Puertas F (2001) Setting of alkali-activated slag cement. Influence of activator nature. Adv Cem Res 13:115–121. https://doi.org/10.1680/ADCR.13.3.115.39288

26. Wang SD, Scrivener KL, Pratt PL (1994) Factors affecting the strength of alkali-activated slag. Cem Concr Res 24:1033–1043. https://doi.org/10.1016/0008-8846(94)90026-4

27. Fernández-Jiménez A, Palomo JG, Puertas F (1999) Alkali-activated slag mortars: mechanical strength behaviour. Cem Concr Res 29:1313–1321. https://doi.org/10.1016/S0008-8846(99)00154-4

28. Jin F, Al-Tabbaa A (2015) Strength and drying shrinkage of slag paste activated by sodium carbonate and reactive MgO. Constr Build Mater 81:58–65. https://doi.org/10.1016/J.CONBUILDMAT.2015.01.082

29. Yuan B, Yu QL, Brouwers HJH (2017) Evaluation of slag characteristics on the reaction kinetics and mechanical properties of $Na_2CO_3$ activated slag. Constr Build Mater 131:334–346. https://doi.org/10.1016/J.CONBUILDMAT.2016.11.074

30. Walling SA, Bernal SA, Gardner LJ et al (2018) Blast furnace slag-$Mg(OH)_2$ cements activated by sodium carbonate. RSC Adv 8:23101–23118. https://doi.org/10.1039/C8RA03717E

31. Bernal SA (2016) Advances in near-neutral salts activation of blast furnace slags. RILEM Tech Lett 1:39. https://doi.org/10.21809/RILEMTECHLETT.V1.8

32. Provis JL, Brice DG, Buchwald A et al (2014) Demonstration projects and applications in building and civil infrastructure. RILEM State Art Rep 13:309–338. https://doi.org/10.1007/978-94-007-7672-2_11/FIGURES/20

33. Provis JL, Duxson P, Kavalerova E et al (2014) Historical aspects and overview. RILEM State Art Rep 13:11–57. https://doi.org/10.1007/978-94-007-7672-2_2/FIGURES/8

34. Long WJ, Tan XW, Xiao BX et al (2019) Effective use of ground waste expanded perlite as green supplementary cementitious material in eco-friendly alkali activated slag composites. J Clean Prod 213:406–414. https://doi.org/10.1016/J.JCLEPRO.2018.12.118

35. Lecomte I, Henrist C, Liégeois M et al (2006) (Micro)-structural comparison between geopolymers, alkali-activated slag cement and Portland cement. J Eur Ceram Soc 26:3789–3797. https://doi.org/10.1016/J.JEURCERAMSOC.2005.12.021

36. Kucharczyk S, Zajac M, Stabler C et al (2019) Structure and reactivity of synthetic $CaO$-$Al_2O_3$-$SiO_2$ glasses. Cem Concr Res 120:77–91. https://doi.org/10.1016/j.cemconres.2019.03.004

37. Król M, Morawska J, Mozgawa W, Pichór W (2014) Low-temperature synthesis of zeolite from perlite waste–Part I: review of methods and phase compositions of resulting products. Mater Sci Poland 32(3):503–513. https://doi.org/10.2478/S13536-014-0216-Y

38. Scrivener K, Snellings R, Lothenbach B (2016) A practical guide to microstructural analysis of cementitious materials, 1st edn. Taylor & Francis Inc, Abingdon-on-Thames

39. Jornson DR, Ross WA (1973) Gaylussite: thermal properties by simultaneous thermal analysis. Am Miner 58:778–784

40. Mozgawa W, Deja J (2009) Spectroscopic studies of alkaline activated slag geopolymers. J Mol Struct 924–926:434–441. https://doi.org/10.1016/J.MOLSTRUC.2008.12.026

41. Garcia-Lodeiro I, Palomo A, Fernández-Jiménez A, Mac-Phee DE (2011) Compatibility studies between N-A-S-H and C-A-S-H gels. Study in the ternary diagram $Na_2O$–$CaO$–$Al_2O_3$–$SiO_2$–$H_2O$. Cem Concr Res 41:923–931. https://doi.org/10.1016/J.CEMCONRES.2011.05.006

42. Puertas F, Torres-Carrasco M (2014) Use of glass waste as an activator in the preparation of alkali-activated slag. Mechanical strength and paste characterisation. Cem Concr Res 57:95–104. https://doi.org/10.1016/J.CEMCONRES.2013.12.005

43. Puertas F, Fernández-Jiménez A, Blanco-Varela MT (2004) Pore solution in alkali-activated slag cement pastes. Relation to the composition and structure of calcium silicate hydrate. Cem Concr Res 34:139–148. https://doi.org/10.1016/S0008-8846(03)00254-0

44. Palacios M, Puertas F (2006) Effect of carbonation on alkali-activated slag paste. J Am Ceram Soc 89:3211–3221. https://doi.org/10.1111/J.1551-2916.2006.01214.X

45. Sitarz M (2011) The structure of simple silicate glasses in the light of Middle Infrared spectroscopy studies. J Non Cryst Solids 357:1603–1608. https://doi.org/10.1016/j.jnoncrysol.2011.01.007

46. Mozgawa W, Sitarz M (2002) Vibrational spectra of aluminosilicate ring structures. J Mol Struct 614:273–279. https://doi.org/10.1016/S0022-2860(02)00261-2

47. Sitarz M, Handke M, Mozgawa W (1999) Calculations of silicooxygen ring vibration frequencies. Spectrochim Acta A Mol Biomol Spectrosc 55:2831–2837. https://doi.org/10.1016/S1386-1425(99)00101-8

48. Wiyantoko B, Kurniawati P, Purbaningtias TE, Fatimah I (2015) Synthesis and characterization of hydrotalcite at different Mg/Al molar ratios. Procedia Chem 17:21–26. https://doi.org/10.1016/J.PROCHE.2015.12.115

49. Trezza MA, Lavat AE (2001) Analysis of the system $3CaO \cdot Al_2O_3$–$CaSO_4 \cdot 2H_2O$–$CaCO_3$–$H_2O$ by FT-IR spectroscopy. Cem Concr Res 31:869–872. https://doi.org/10.1016/S0008-8846(01)00502-6

50. Partyka J, Leśniak M (2016) Raman and infrared spectroscopy study on structure and microstructure of glass–ceramic materials from $SiO_2$–$Al_2O_3$–$Na_2O$–$K_2O$–$CaO$ system modified by variable molar ratio of $SiO_2/Al_2O_3$. Spectrochim Acta A Mol Biomol Spectrosc 152:82–91. https://doi.org/10.1016/j.saa.2015.07.045

51. Ukrainczyk N, Matusinovic T, Kurajica S et al (2007) Dehydration of a layered double hydroxide—$C_2AH_8$. Thermochim Acta 464:7–15. https://doi.org/10.1016/j.tca.2007.07.022